# Chapter IV

## Nanoscale gadolinium oxyfluoride ($Gd_4O_3F_6$) systems with $Eu^{3+}$ inclusion

Nanoscale rare –earth (RE) materials have drawn worldwide attention for their immense potential in the field of light emitting diodes (LED), flat panel displays and solar energy converters [1-3]. Presently, in order to improve biomedical imaging and contrast, special emphasis is also given to nanosized luminescent RE candidates [4,5]. The RE doped fluorides are well known luminescent hosts, as they have low phonon energy and consequently, display luminescence due to the low probability of multiphonon non-radiative processes [6,7]. Moreover, lanthanide oxyfluoride, while exhibiting high iconicity, thermal and chemical stability can act as a suitable host material as it could easily accommodate luminescent lanthanide ions as dopants. Earlier most of the studies were focused to synthesize $Eu^{3+}$ (or $Tb^{3+}$) doped lanthanum, gadolinium and yttrium oxyfluorides [8,9] in bulk form, or in thin film form [10]. It has also become possible to synthesize $Eu^{3+}$ doped gadolinium oxyfluoride ($Gd_4O_3F_6$) nanoparticles in an amorphous media, like silica matrix [11]. From application point of view, upconversion responses of $Er^{3+}$, $Tm^{3+}$, $Yb^{3+}$ doped $Gd_4O_3F_6$ nanoparticles have been evaluated qualitatively [12]. As for $Gd_4O_3F_6$ system doped with $Eu^{3+}$ ions, possibility of a modified crystal structure along with manifested luminescence characteristics has also been discussed in a recent work [13]. In the past, sol gel [13, 14] and hydrothermal [15, 16] techniques have been employed to synthesize RE oxyfluorides. Often, the methods either rely on annealing of $REF_3$ in air atmosphere or allow a solid-state reaction between $RE_2O_3$ and $REF_3$ or $NH_4F$. While every method has its own advantage and shortcoming, a reliable route that avoids punitive reaction environment and complicated strategies is generally accepted by the research community for large scale production.

The present study highlights production of a matrix-free, RE oxyfluoride nanoscale system e.g., $Eu^{3+}$ doped $Gd_4O_3F_6$ (GOF) derived through a modified Pechini method. The microstructural, radiative emission response, vibrational, and Raman active modes are discussed.

## 4.1 Synthesis of $Eu^{3+}$ doped $Gd_4O_3F_6$ nanosystems

In order to synthesize nanoscale GOF system, a modified Pechini's method has been adopted [13]. In a typical procedure, 0.28 g of bulk $Gd_2O_3$ (Otto, 99.9% purity) is first dispersed in 35 ml deionized water followed by addition of an appropriate amount of dil. $HNO_3$ and until a clear sol is obtained. Then 3.6 g of citric acid ($C_6H_8O_7$, CDH, 99% purity) and 0.6 ml of ethylene glycol ($C_2H_6O_2$, Merck, 99% purity)) was allowed to reflux with the sol. To inhibit precipitation, citric acid was used in excess amount. During rigorous stirring, an aqueous solution of ammonium fluoride ($NH_4F$, Merck, 99% purity) is gently mixed with the aforesaid solution. Next, the as-prepared sol is cleansed several times, first with distilled water and then with ethanol, and subsequently oven-dried at a temperature of 70$^oC$. Finally, the prepared precursor is annealed at a temperature of 500°C for 2 h. For synthesizing $Eu^{3+}$ doped $Gd_4O_3F_6$ product, an appropriate amount of europium oxide ($Eu_2O_3$, Otto, 99.9% purity) has been added to the chamber during the initial step of the reaction, while rest of the steps remained unchanged. In order to synthesize GOF nanosystem with 3%, 5% and 7% Eu doping concentration, a proportionate amount of $Eu_2O_3$, for instance, 0.0084 g, 0.0075 g and 0.0196 g are taken with the bulk $Gd_2O_3$ powder. The purpose of RE doping was to manifest optical and vibrational characteristics with regard to pure GOF system.

## 4.2 Microstructural and morphological analyses of $Gd_4O_3F_6$ nanosystems

The XRD patterns of undoped and $Eu^{3+}$ doped $Gd_4O_3F_6$ nanoparticles are shown in Figure 4.1. The four peaks located at ~ 27.65°, 32.30°, 46.20° and 54.35° corresponded to (111), (002), (202) and (311) crystallographic planes (JCPDS No. 76-0155) [12]. With a preferred crystallographic orientation along (111) plane, the diffractograms represent a tetragonal crystal structure of $Gd_4O_3F_6$ system [12]. An appreciable peak shifting was noticeable in case of $Eu^{3+}$ doped GOF nanosystems which indicate possible change in strain and lattice parameter after incorporation of $Eu^{3+}$ into GOF lattice [17]. The average crystallite size ($d$) can be calculated by

employing single line fitting of the preferred (111) peak and using the Scherrer expression: $d = 0.91\lambda/\beta \cos\theta$, where $\beta$ is the full width at half maxima (FWHM), $\theta$ is the diffraction angle in degree and λ is the wavelength of X-rays (1.543 Å). The lattice parameters are computed using a formula that relates inter-planar spacing and parameters satisfying 1st order Bragg's diffraction ($2d \sin\theta = \lambda$) and exhibiting a tetragonal symmetry [12]. We write,

$$\frac{1}{d^2_{hkl}} = \frac{h^2+k^2}{a^2} + \frac{l^2}{c^2} \quad (4.1)$$

where $d_{hkl}$ is the Bragg diffraction spacing for the ($hkl$) plane ($h$, $k$ and $l$ are Miller indices), $a$ (=$b$) and $c$ are the unit parameters of the tetragonal crystal structure. The calculated values of average crystallite size and lattice parameters are presented in Table 4.1.

To quantify the degree of orientation normally Lotgering factor is introduced. The Lotgering factor, $L_F$ is based on the evaluation between the measured XRD patterns and that expected for randomly oriented powders. In reference to a specific crystallographic plane, the $L_F$ is defined as [18]:

$$L_F(hkl) = \frac{P(hkl)-P_o(hkl)}{1-P_o(hkl)} \quad (4.2)$$

Here $P(hkl)$ is the ratio of the XRD intensity of the ($hkl$) reflection over the scanned range, and $P_o(hkl)$ is an equivalent value for a randomly oriented $Gd_4O_3F_6$ system (JCPDS file No 76-0155) [12]. The $L_F$ varies from 0, for non-orientation case to 1 for complete orientation. In reference to (111) peaks, the Lotgering factor is found to increase from 0.20 to 0.48 with increasing $Eu^{3+}$ concentration (Table 4.1). Inclusion of $Eu^{3+}$ ions essentially orient grains in a more effective manner, resulting in a higher $L_F$ value.

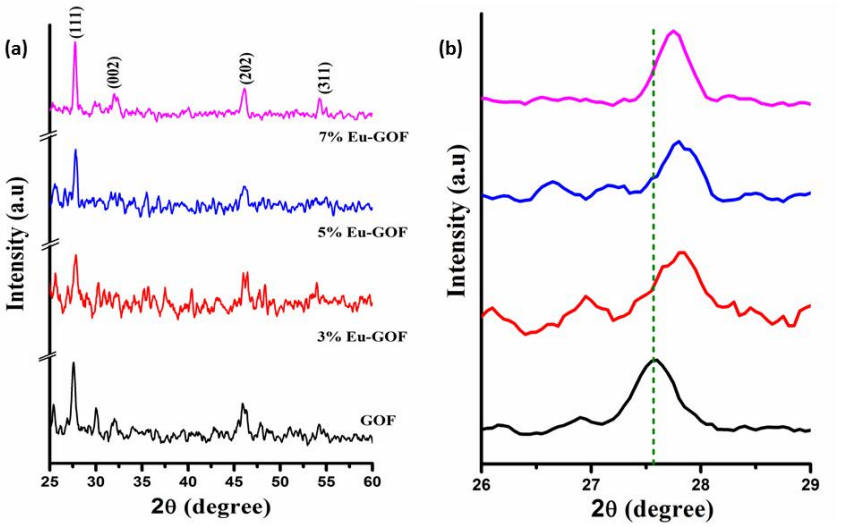


Figure 4.1: (a) XRD patterns of undoped and $Eu^{3+}$ doped $Gd_4O_3F_6$ nanosystems, (b) zoomed version of XRD patterns to highlight peak-shifting with $Eu^{3+}$ doping.

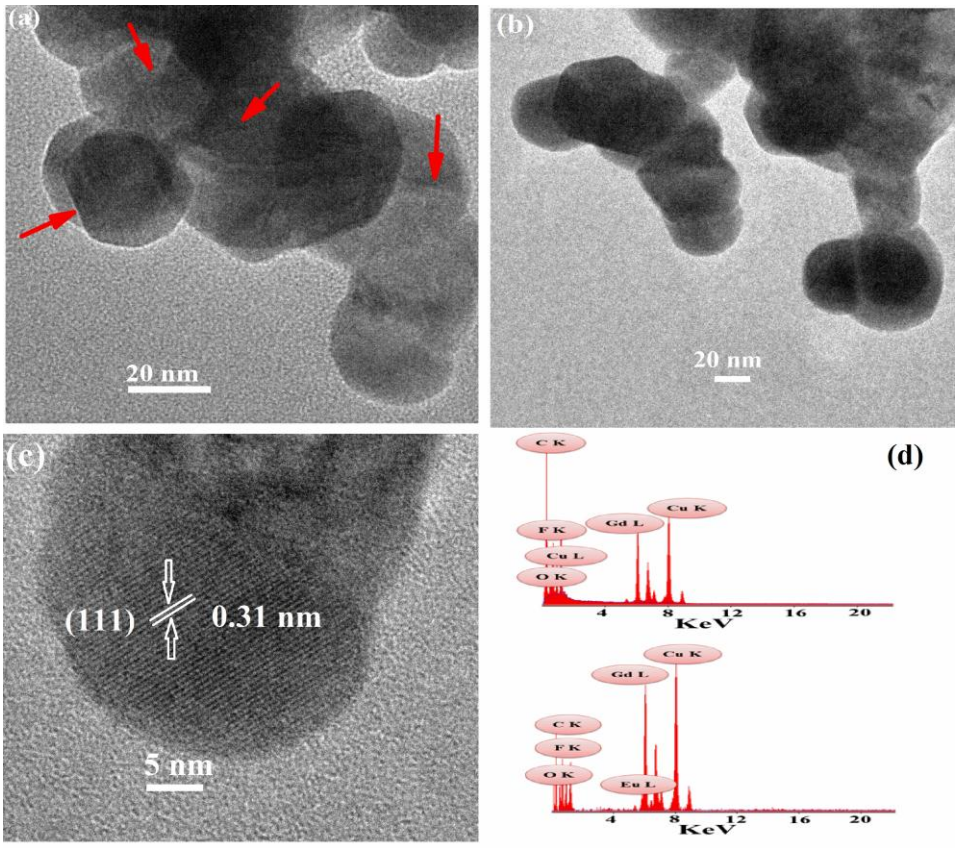


Figure 4.2: (a) HRTEM images of $Gd_4O_3F_6$ nanoparticles, and (b) 7% $Eu^{3+}$ doped GOF sample (c) an isolated GOF nanoparticle depicting lattice fringe, (d) EDX patterns of (lower) undoped and (upper) 7% $Eu^{3+}$ doped GOF specimens.

Table 4.1: Physical parameters derived through XRD analyses of $Eu^{3+}$:$Gd_4O_3F_6$ nanosystems

| Eu (%) | Average crystallite size ,*d* (nm) | Lattice parameter (Å) | | | Lotgering factor (*F*) |
|---|---|---|---|---|---|
| | | *a* | *c* | *c/a* | |
| 0 | 25.01 | 5.54 | 5.57 | 1.005 | 0.20 |
| 3 | 21.17 | 5.48 | 5.58 | 1.018 | 0.22 |
| 5 | 22.12 | 5.50 | 5.58 | 1.014 | 0.24 |
| 7 | 26 | 5.57 | 5.53 | 0.99 | 0.48 |

The TEM images of undoped and 7% $Eu^{3+}$ doped $Gd_4O_3F_6$ nanosystems are shown in Figure 4.2(a) and (b). Both the undoped and doped systems comprise of spheroidal nanoparticles with occasional instances of sharp edges, indicated by short arrows. The average dimension of the GOF nanoparticles is ~30-45 nm. Figure 3.2(c) depicts an isolated nanoparticle with prominent lattice fringe pattern. The inter-planar spacing is estimated to be ~0.31 nm and corresponded to (111) plane of the tetragonal structure of $Gd_4O_3F_6$ system. The EDX patterns of the undoped and 7% $Eu^{3+}$ doped nanosystems are presented in Figure 4.2(d). Apart from signals corresponding to Gd, O, and F elements; a peak due to trace element Eu can also be seen for the doped GOF system. A prominent peak due to Cu is believed to have arisen due to a supporting copper grid for EDX measurements. Nevertheless, all other prime peaks emanating from the specimen are distinctly observable.

### 4.3 Optical absorption and photoluminescence responses of GOF systems

Figure 4.3(a) shows the optical absorption spectra of $Gd_4O_3F_6$ nanosystems. As can be found, the absorption spectra of the undoped and $Eu^{3+}$ doped GOF nanoparticles depict a broad absorption feature over a wide range of wavelength. The absorption peak at ~248 nm is due to one of the transition of $Gd^{3+}$

corresponding to ${}^8S_{7/2} \rightarrow {}^6I_{j/2}$ multiplets (where, $j$= 9,12,13,15 and 17). To be specific, the $Eu^{3+}$ doped nanosystems are characterized by two broad peak maxima located at ~252 and ~590 nm. The peak at ~590 nm can be assigned to the magnetically driven ${}^5D_0 \rightarrow {}^7F_1$ transitions [19]. It may be noted that, $Gd^{3+}$ has [Xe] $4f^7$ configuration, which means that it has half-filled shells and having a ${}^8S_{7/2}$ ground state [20]. The energy absorption in Gd is mediated via transition of $4f$ electrons to $5d$ level. The seven electrons in $4f$ orbitals of Gd have as many as 3432 multiplets and the ground state is ${}^8S_{7/2}$. Among these multiplets the low lying multiplet above the ground state is ${}^6P_{7/2}$ [20]. While undoped GOF gives nearly featureless characteristics over a broad spectrum, inclusion of $Eu^{3+}$ ions into GOF host offer distinct absorption features owing to introduction of localized states. The individual absorption bands, that illustrate strong absorption signature, can also be identified in the first derivative spectra (Figure 4. 3(b)).

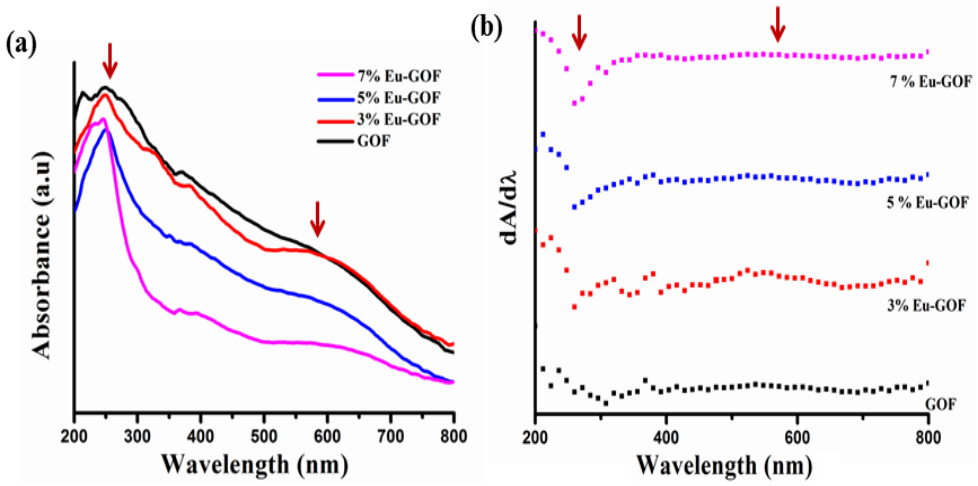


Figure 4.3: (a) Optical absorption spectra of undoped and $Eu^{3+}$ doped $Gd_4O_3F_6$ nanosystems, (b) corresponding first derivative spectra of the samples.

Figure 4.4(a) shows the emission spectra of $Gd_4O_3F_6$ nanoscale systems without and with inclusion of $Eu^{3+}$ ions (3, 5, and 7%). The luminescence data is acquired at an excitation wavelength, $\lambda_{ex}$ = 400 nm. Upon excitation, strong emission response has been observed at ~ 490 nm, 572 nm, 595 nm and 613 nm which can be ascribed

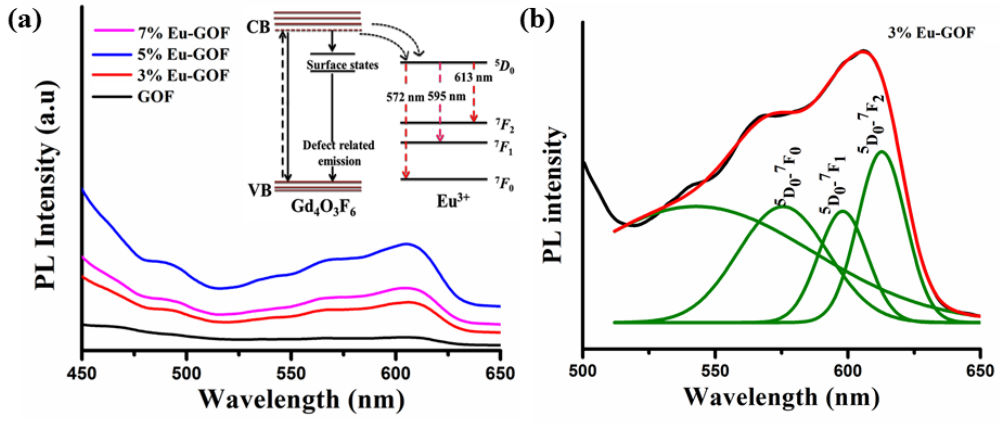


Figure 4.4: (a) PL emission spectra of undoped and $Eu^{3+}$ doped GOF samples. The schematic diagram on radiative transitions is illustrated in figure inset. The deconvoluted PL spectra of 3% Eu doped $Gd_4O_3F_6$ nanosystem is shown in (b).

to *D-F* transition of $Eu^{3+}$ ions. The peak positions are identified through multi-peak Gaussian fitting of the overall spectrum. In this process, the area under the experimental curve is kept equal to the area under the empirical curve, which is nothing but the sum total of the area under each of the deconvoluted curves. A normalized Gaussian fitting of 3% $Eu^{3+}$ doped GOF nanosystem can be found in Figure 4(b). The ~490 nm peak is assigned to the higher energy level (*f-f*) transitions of $Eu^{3+}$[19]. The respective peak maxima at ~572 nm, 595 nm and 613 nm corresponded to $^5D_0 \rightarrow ^7F_0$, $^5D_0 \rightarrow ^7F_1$, $^5D_0 \rightarrow ^7F_2$ transitions of $Eu^{3+}$ ions [19]. The schematic energy diagram and the possible transitions are illustrated schematically, in Fig. 4(c). The transition, $^5D_0 \rightarrow ^7F_1$ originates from the magnetic dipole transition and it is permitted only on the condition that the $Eu^{3+}$ ion occupies a site with an inversion center and is not dependent on the site symmetry. The $^5D_0 \rightarrow ^7F_2$ transition originates from the electric dipole transition and it is allowed only when $Eu^{3+}$ is occupied in low symmetries without any center of inversion and consequently, it is hypersensitive to the environmental effect. The intensities of $^5D_0 \rightarrow ^7F_1$ and $^5D_0 \rightarrow ^7F_2$ mediated emissions, for different $Eu^{3+}$ concentrations, are computed from the integrated area under each of the deconvoluted curves, e.g., in the range of 572- 625 nm and 586-638 nm;

respectively. In case of a higher doping level (7% $Eu^{3+}$), the 613 nm red emission peak decreases substantially owing to concentration quenching. We anticipate that, at a relatively low doping the concentration quenching effect is insignificant because of the fact that, (i) $Eu^{3+}$ could easily occupy $Gd^{3+}$ sites of $Gd_4O_3F_6$ lattice owing to similar ionic radii of both the ion types, (ii) the Eu-Eu interionic distance is fairly large to retain radiative events. The quenching effect comes from the cross relaxation among $Eu^{3+}$ ions which increases with decreasing distance between $Eu^{3+}$ -$Eu^{3+}$ ions [19]. The asymmetric ratio ($A_{sy}$) which is defined as the ratio of integrated intensities of electric dipole transition to the magnetic dipole transition is found to drop from 1.36 to 1.25 on increasing concentration of $Eu^{3+}$ doping (Table 4.2). A suppressed value of $A_{sy}$ at a higher doping level may have arisen due to concentration quenching effect.

To assess the influence of local environment and bonding in the proximity of a RE ion, Judd-Ofelt (J-O) intensity parameter, $\Omega_J$ ($J$=2) has been calculated [21]. Essentially, $\Omega_2$ characterizes a short range parameter that gives information about the degree of covalency and polarizability of chemical environment experienced by the RE ions. The rate radiative emission and intensity of emission corresponding to $^5D_0 \rightarrow {}^7F_2$ transition can be formulated as [21]:

$$A_{0-J}=A_{0-1}\frac{I_{0-J}}{I_{0-1}}\frac{h\nu_{0-1}}{h\nu_{0-J}}\ , \qquad (4.3)$$

where $I_{0-1}$ and $I_{0-J}$ are integral intensities for $^5D_0 \rightarrow {}^7F_1$ (pure magnetic dipole) and $^5D_0 \rightarrow {}^7F_J$ transitions and $h\nu_{0-1}$ and $h\nu_{0-J}$ are associated energies (in $cm^{-1}$); respectively. Note that magnetic dipole transition $^5D_0 \rightarrow {}^7F_1$ is not much affected by the local environment and its transition rate is constant with an approximate value of 50 $s^{-1}$. The electric dipole transitions $^5D_0 \rightarrow {}^7F_J$ ($J$=2,4 and 6) can be expressed in the following relation [21]

$$A_{0-J}=\frac{64\pi^4 e^2 K^3}{3h(2J+1)}\frac{\mu(\ \mu^2\ +2)^2}{9}\sum \Omega_\lambda < \psi J|U^\lambda|\psi' J' >^2 \qquad (4.4)$$

Here $\mu$ is the refractive index of the medium, $e$ is the electronic charge, $K$ is the transition energy of electric dipole transitions in $cm^{-1}$, $\Omega_\lambda$ is the J-O intensity parameter and $< \psi J|U^\lambda|\psi' J' >^2$ values are the squared reduced matrix elements whose values are 0.0032 and 0.0023 for $J' = 2$ and 4 respectively[21]. A relatively high value of $\Omega_2$ in case of 3% $Eu^{3+}$ doped GOF sample indicate a strong asymmetric environment of the dopant ions in the host (Table 4.2). Note that, Judd-Ofelt parameters are not constants and are dependent on the processing temperature, particle dimension and nature of Eu3+ doping. The parameter $\Omega_2$ is related to the covalency or structural changes in the vicinity of Eu3+ ion which is a short range effect. A large value of ($\Omega_2$) intensity parameter is an indication of high covalence of the metal-ligand bonds. The $\Omega_2$ value in our case is small compared to the reported values, signifying a relatively less asymmetric environment around $Eu^{3+}$ in the GOF host lattice.

It is the order of the J-O parameter which matters not magnitude, the latter might alter due to sample processing conditions and the reason described above.

Table 4.2: Judd-Ofelt intensity parameters ($\Omega_2$) and asymmetric parameters obtained from luminescence spectra.

| Samples | $\Omega_2$ ($10^{-20}$ $cm^2$) | asymmetric ratio, $A_{sy}$ |
|---|---|---|
| 3%$Eu^{3+}$:$Gd_4O_3F_6$ | 3.21 | 1.36 |
| 5%$Eu^{3+}$:$Gd_4O_3F_6$ | 2.91 | 1.30 |
| 7%$Eu^{3+}$:$Gd_4O_3F_6$ | 2.65 | 1.25 |

## 4.4 IR active molecular vibrational characteristics

The FTIR spectra of the undoped and $Eu^{3+}$ doped $Gd_4O_3F_6$ nanoparticles are shown in Figure 4.5. The data acquired within a wavenumber range 400 to 4000 $cm^{-1}$ characterize several IR active bands resolved at ~452 $cm^{-1}$, 512 $cm^{-1}$, 734 $cm^{-1}$, 1016 $cm^{-1}$, 1317 $cm^{-1}$, 1640 $cm^{-1}$, 2915 $cm^{-1}$ and 3432 $cm^{-1}$. The prominent bands at ~3432 $cm^{-1}$ and 1640 $cm^{-1}$ are attributed to the O-H stretching vibration and bending of water molecules [22]. The band at ~2915 $cm^{-1}$ can be attributed to the asymmetric vibration of $-CH_2$, whereas dips at ~1317 $cm^{-1}$

and 1016 $cm^{-1}$ are assigned to vibration of C–O bonds. The low frequency bands at ~512 $cm^{-1}$ and ~452 $cm^{-1}$ are believed to be caused by the stretching vibration of Gd-O bonds within the GOF system [13]. Moreover, the band at ~734 $cm^{-1}$ is believed to have appeared due to the C-O stretching vibration of the sample. For clarity, the Gd-O vibration related peaks are highlighted as inset of Figure 4.5.

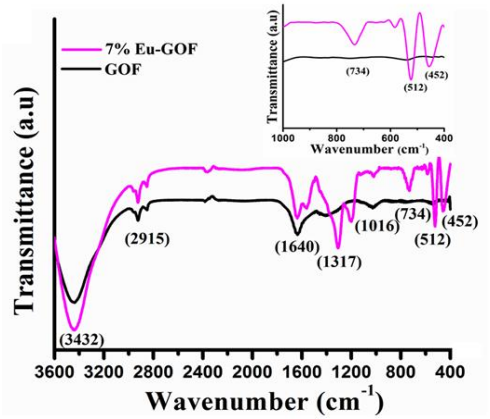


Figure 4.5: FTIR spectra of undoped and 7% $Eu^{3+}$ doped $Gd_4O_3F_6$ nanosystems

## 4.5 Manifestation of Raman active modes

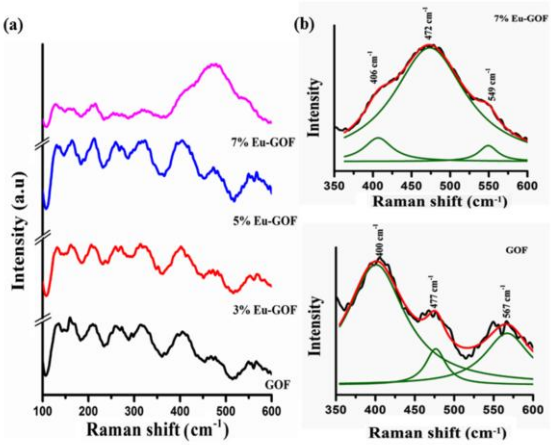


Figure 4.6: (a) Raman spectra of un-doped and $Eu^{3+}$ doped $Gd_4O_3F_6$ nanosystems, (b) deconvoluted Raman spectra of undoped and 7% $Eu^{3+}$ doped GOF nanosystems.

Raman spectroscopy is a powerful non-invasive technique based on inelastic scattering of light with molecular systems. Raman active vibrational modes are exploited through a high precision Raman spectrometer (Horiba Jobin Vyon,

LabRam HR) and employing a red diode laser ($\lambda_{ex}$= 632 nm) as the excitation source. In general, IR active modes are not Raman active and therefore, the latter finds a special place to uncover lattice vibrational characteristics of the material under study. According to the group theory, the normal lattice vibration at the $\Gamma$ point of the Brillouin zone can be formulated as [23]:

$$\Gamma_{tg}=A_{1g}+2B_{1g}+2A_{2u}+3E_g+2E_u \quad (4.5)$$

On the basis of group theory selection rules in the RE oxyfluorides, $A_{1g}+2B_{1g}+3E_g$ are Raman active, but $2A_{2u}+2E_u$ are IR active modes [23]. The Raman spectra of undoped and $Eu^{3+}$ doped $Gd_4O_3F_6$ nanoparticles are shown in Figure 4.6(a). Eight distinct peaks, located at a Raman shift of ~128 $cm^{-1}$, 165 $cm^{-1}$, 210 $cm^{-1}$, 266 $cm^{-1}$, 319 $cm^{-1}$, 407 $cm^{-1}$, 481 $cm^{-1}$ and 566 $cm^{-1}$ can be witnessed in the spectra. The first four peaks (at ~128, 165, 210 and 266 $cm^{-1}$) are attributed to the movement of heavy Gd-Gd pairs as predicted in an earlier work [13]. A similar Raman signature has been also detected for a LaOF system possessing tetragonal crystal structure [23]. Notably, the peak at ~477 and 567 $cm^{-1}$ can account for phononic vibration of the Gd-O groups [13]. From the Raman spectra we also noticed that the peak at ~477 $cm^{-1}$ shifts to a higher wavenumber value with increase in concentration of the $Eu^{3+}$ ions and up to 5% $Eu^{3+}$doping level. At a 7% doping, the peak again downshifts to ~472 $cm^{-1}$ but ensuring a much improved signal strength (Figure 4.6(b)). Moreover, ~567 $cm^{-1}$ peak of undoped GOF system is shifted to ~549 $cm^{-1}$. At a higher doping level, we anticipate involvement of surface phonon modes exhibited by the symmetrically located dopants in the GOF host. In fact, the shifting of the Raman peak towards a higher frequency side is believed to be due to the reduction of particle size (see also XRD analysis on the trend of crystallite size with doping, Table 4.1). According to the Heisenberg's uncertainty principle, we have [24]

$$\Delta x \Delta p \geq \hbar/2, \quad (4.6)$$

where $\Delta x$ is the particle size, $\Delta p$ is phonon momentum distribution and $\hbar$ is the reduced Planck's constant. With particle size reduction, phonon confinement and hence phonon energy tend to upsurge significantly. This results in Raman peak broadening of the scattered phonons according to the law of conservation of momenta [24]. From the XRD analysis, the average crystallite size of the GOF nanoparticles is found to decrease from ~25 nm to 22 nm with increasing $Eu^{3+}$ doping from 0 to 5%. Conversely, the 7% $Eu^{3+}$ doped GOF system has a larger crystallite size (~26 nm) and much improved Raman band. In semiconductor oxide nanomaterials, the peak shift and line broadening aspect is normally assigned to crystal defects, oxygen vacancies and inhomogeneous strain [25]. In the present case, the manifested Raman intensity and peak shift in certain wavenumber region can be ascribed to local distortion of crystal structure of GOF with incorporation $Eu^{3+}$ ions [23]. The symmetric environment provided by the dopants could support confinement of surface optic phonons, resulting in the intense Raman band.

## 4.5 Concluding remarks

Nanocrystalline undoped and $Eu^{3+}$ doped $Gd_4O_3F_6$ are synthesized by a modified Pechini's method. The Lotgering factor which accounts for extent of crystallite orientation along the preferred plane is adequately enhanced for a higher doping level. The orange emission at ~595 nm and red emission at ~613 nm are assigned to $^5D_0 \rightarrow {}^7F_1$ and $^5D_0 \rightarrow {}^7F_2$ transition; respectively. Both J-O parameter and asymmetric ratio fall with increasing $Eu^{3+}$ doping. The electrically driven $^5D_0 \rightarrow {}^7F_2$ being hypersensitive to environment is expected to get suppressed by concentration quenching at 7% $Eu^{3+}$ doping. The low frequency Gd-O bonding is revealed in the FTIR spectra between 450-550 $cm^{-1}$. Raman active modes of high $Eu^{3+}$ doped GOF sample reveal intense peaks owing to involvement of surface optic modes.

## References

[1] Bachmann, V., Ronda, C., and Meijerink, A. Temperature Quenching of Yellow $Ce^{3+}$ Luminescence in YAG:Ce. *Chemistry of Materials,* 21**:**2077-2084, 2009.

[2] van der Ende, B.M., Aarts, L., and Meijerink, A. Lanthanide ions as spectral converters for solar cells. *Physical Chemistry Chemical Physics*, 11:11081-11095, 2009.

[3] Reisfeld, R. New developments in luminescence for solar energy utilization. *Optical Materials,* 32: 850-856, 2010.

[4] Vetrone, F., Naccache, R., Fuente, A. J. de la., Rodríguez, F. S., Castro, A. B., Rodriguez, E.M., Jaque, D., Solé, J. G., and Capobianco, J.A. Intracellular imaging of HeLa cells by non-functionalized $NaYF_4$ : $Er^{3+}$, $Yb^{3+}$ upconverting nanoparticles. *Nanoscale*, 2:495-498, 2010.

[5] Kumar, R., Nyk, M., Ohulchanskyy, T.Y., Flask, C.A., and Prasad, P.N. Combined optical and MR bioimaging using rare earth ion doped $NaYF_4$ nanocrystals. *Advance Function Materials,* 19: 853-859, 2009.

[6] Hölsä, J., Piriou, B., and Räsänen, M. IR- and Raman-active normal vibrations of rare earth oxyiluorides, REOF; RE=Y, La, and Gd. *Spectrochimica Acta*, 49A: 465-470, 1993.

[7] Cornacchia, F., Lieto, A. Di., and Tonelli, M. $LiGdF_4$:$Tm^{3+}$: spectroscopy and diode-pumped laser experiments. *Applied Physics B laser and optics,* 96: 363-368, 2009.

[8] Hölsä, J., and Kestilä, E. Study of the crystal field effect in REOF:$Eu^{3+}$ (RE=La, Gd and Y) using optical spectroscopy and X-ray powder diffraction. *Journal of Alloys and Compounds,* 225: 89-94,1995.

[9] Fidancev, E. A., Hölsä, J., Krupa, J.-C., and Lastusaari, M. Crystal fields in ROF:$Tb^{3+}$ (R = La, Gd). *Journal of Alloys and Compounds,*380: 303-309,2004.

[10] Armelao, L., Bottaro, G., Bruno, G., Losurdo, M., Pascolini, M., Soini, E., and Tondello, E. Lanthanum Oxyfluoride Sol-gel Thin Films by a Simple Single-Source Precursor Route. *Journal of Physical Chemistry C,*112:14508-14512, 2008.

[11] Fujihara, S., Koji, S., and Kimura, T. Structure and optical properties of (Gd,Eu)$F_3$-nanocrystallized sol–gel silica films. *Journal of Materials Chemistry,* 14: 1331-1335, 2004.

[12] Passuello, T., Piccinelli, F., Pedroni, M., Bettinelli, M., Mangiarini, F., Naccache, R., Vetrone, F., Capobianco, J.A., and Speghini, A. White light upconversion of nanocrystalline Er/Tm/Yb doped tetragonal $Gd_4O_3F_6$. *Optical Materials,* 33: 643-646, 2011.

[13] Grzyb, T., Wiglusz, R. J., Nagirnyi, V., Kotlov ,A., and Lis, S. Revised crystal structure and luminescent properties of gadolinium oxyfluoride $Gd_4O_3F_6$ doped with $Eu^{3+}$ ions. *Dalton Transactions*, 43:6925-6934,2014.

[14] Hölsä, J. Effect of non-stoichiometry on the luminescence properties of lanthanum oxyfluorides. *Acta Chemica Scandinavica ,* 45:583-587, 1991.

[15] Du, Y.-P., Zhang, Y.-W., Sun, L.-D., and Yan, C.-H. Luminescent Monodisperse Nanocrystals of Lanthanide Oxyfluorides Synthesized from Trifluoroacetate Precursors in High-Boiling Solvents. *Journal of Physical Chemistry C,*112: 405-415, 2008.

[16] Du, Y.-P., Zhang, Y.-W., Yan, Z.-G., Sun, L.-D., and Yan, C.-H. Highly Luminescent Self-Organized Sub-2-nm EuOF Nanowires. *Journal of American Chemical Society*, 131: 16364–16365, 2009.

[17] Archana, P. S., Gupta, A., Yusoff, M. M., and Jose, R. Charge transport in zirconium doped anatase nanowires dye-sensitized solar cells: Trade-off between lattice strain and photovoltaic parameters. *Applied physics letter,* 105:153901-5 ,2014.

[18] Lotgering, F. K. Topotactical reactions with ferromagnetic oxides having hexagonal crystal structures-I. *Journal of Inorganic and Nuclear Chemistry,* 9: 113-123, 1959.

[19] Ningthoujam , R. S., Shukla, R., Vatsa, R. K., Duppel, V., Kienle, L., and Tyagi, A. K. $Gd_2O_3$ : $Eu^{3+}$ particles prepared by glycine-nitrate combustion: Phase, concentration, annealing, and luminescence studies. *Journal of Applied Physics* ,105: 084304-7,2009.

[20] Rahman, A.T.M., Vasilev, K., and Majewski, P. Ultra small $Gd_2O_3$ nanoparticles: Absorption and emission properties. *Journal of Colloid and Interface Science,* 354: 592-596 2011.

[21] Liu, Li., and Chen, X. Energy levels, fluorescence lifetime and Judd–Ofelt parameters of $Eu^{3+}$ in $Gd_2O_3$ Nanocrystals. *Nanotechnology,* 18:255704 (8pp) ,2007.

[22] Du, P., Song, L., Xiong, J., Xi, Z., Jin, D., and Wang, L. Preparation and the luminescent properties of $Tb^{3+}$ doped $Gd_2O_3$ fluorescent nanofibers via electrospinning. *Nanotechnology*, 22: 035602(5pp), 2011.

[23] Hölsä, J., Säilynoja, E., Rahiala, H., and Valkonen, J. Characterization of the non-stoichiometry in lanthanum oxyfluoride by FT-IR absorption, Raman scattering, X-ray powder diffraction and thermal analysis. *Polyhedron,* 16: 3421-3427,1997.

[24] Choi, H.C., Jung, Y. M., and Kim, S. B. Size effects in the Raman spectra of $TiO_2$ nanoparticles. *Vibrational Spectroscopy*, 37: 33-38, 2005.

[25] Sahoo, S., Arora, A. K., and Sridharan, V. Raman Line Shapes of Optical Phonons of Different Symmetries in Anatase $TiO_2$ Nanocrystals. *Journal of Physical Chemistry C,* 113: 16927-16933,2009.